Alma Mater Studiorum Università di Bologna
Archivio istituzionale della ricerca

Intracellular distribution and stability of a luminescent rhenium(i) tricarbonyl tetrazolato complex using epifluorescence microscopy in conjunction with X-ray fluorescence imaging

Intracellular distribution and stability of a luminescent rhenium(I) tricarbonyl tetrazolato complex using confocal fluorescence microscopy in conjunction with XFM imaging.

Jason L. Wedding[1], Hugh H. Harris[a], Christie A. Bader[2], Sally E. Plush[b], Rachel Mak[3], Massimiliano Massi[4], Douglas A. Brooks[5], Barry Lai[6], Stefan Vogt[7], Melissa V. Werrett,[d] Peter V. Simpson,[d] Brian W. Skelton,[e] Stefano Stagni[f]

Abstract

Optical fluorescence microscopy was used in conjunction with X-ray fluorescence microscopy to monitor the stability and intracellular distribution of the luminescent rhenium(I) complex *fac*-[Re(CO)$_3$(phen)L], where phen = 1,10-phenathroline and L = 5-(4-iodophenyl)tetrazolato, in 22Rv1 cells. The rhenium complex showed no signs of ancillary ligand dissociation, a conclusion based on data obtained via X-ray fluorescence imaging aligning iodine and rhenium distributions. A diffuse reticular localisation was detected for the complex, in the nuclear/perinuclear region of cells, by either optical or X-ray fluorescence techniques. X-ray fluorescence also showed that the **Re-I** complex disrupted the homeostasis of some biologically relevant elements, such as chlorine, potassium and zinc.

Introduction

Interest and advancement of coordinated group VII elements, such as rhenium and technetium, has been largely due to their application as radionuclides in the development of radiopharmaceuticals[1-5] and as optical dyes for cellular imaging in microscopy.[6-9] The ability to incorporate these radionuclides into tracer molecules has been at the forefront in developing diagnostic

[1] School of Physical Sciences, The University of Adelaide, North Terrace, Adelaide, South Australia, 5005, Australia. E-mail: Hugh.Harris@adelaide.edu.au Fax.: +61 8 8313 4380 Tel.: +61 8 8313 5060

[2] School of Pharmacy and Medical Sciences, University of South Australia, City East – Central Campus, Adelaide, South Australia, 5005, Australia. E-mail: Sally.Plush@unisa.edu.au Fax.: +61 8 8302 2389 Tel.: +61 8 8302 2586

[3] Department of Chemistry, Faculty of Science, The University of Sydney, Sydney, New South Wales, 2006, Australia. E-mail: Rachel.Mak@sydney.edu.au Fax.: +61 2 9351 3329 Tel.: +61 2 9351 7600

[4] Department of Chemistry, Faculty of Science and Engineering, Curtin University, Bentley Campus, Perth, Western Australia, 6102, Australia. E-mail: M.Massi@curtin.edu.au Fax.: +61 8 9266 2300 Tel.: +61 8 9266 2838

[5] School of Pharmacy and Medical Sciences, University of South Australia, City East – Central Campus, Adelaide, South Australia, 5005, Australia. E-mail: Doug.Brooks@unisa.edu.au Fax.: +61 8 8302 1087 Tel.: +61 8 8302 1229

[6] Argonne National Laboratory, 9700 Cass Ave, Lemont, IL 60439, USA. E-mail: blai@aps.anl.gov Tel.: +1 630 252 6405

[7] Argonne National Laboratory, 9700 Cass Ave, Lemont, IL 60439, USA. E-mail: vogt@aps.anl.gov Tel.: +1 630 252 3071

[e] Centre for Microscopy, Characterisation and Analysis, University of Western Australia, Crawley 6009 WA, Australia.

[f] Department of Industrial Chemistry "Toso Montanari" – University of Bologna, viale del Risorgimento 4, Bologna 40136, Italy.

radiopharmaceuticals.[10] [99mTc] has become a popular choice, being used in over 85% of diagnostic scans every year, due to its medicinally appropriate half-life, wide range of compatible ligands to form stable complexes and low bioaccumulation rates in patients.[3,6,10,11] Luminescent metal complexes of rhenium(I), ruthenium(II) and iridium(III) have found considerable application as luminescent imaging agents due to their favorable photophysical properties.[5-7,12,13] In particular, their large Stokes shifts prevents concentration quenching phenomena and also, along with their long excited state lifetime, allows for easier discrimination from background autofluorescence. Furthermore, chemical design can render these complexes photostable, thus preventing fast bleaching upon excitation. Bioconjugation of these complexes to biological vectors (such as avidin or octreotide) has been successfully employed to confer biological specificity in cell lines, including specific organelles, after internalization.[2,4,6-8]

Rhenium[14,15] and iridium[2,16,17] complexes have already been shown to be useful as cellular imaging agents due to their favorable intracellular localizations and organelle targeting,[18] and offer the possibility of combining their functions as fluorescence microscopy imaging agents with *in vivo* radio-imaging.[5,19-22] For example rhenium(I) is used as a "cold", or non-radioactive, [99mtechnicium] chemical analogue, thereby allowing for insight into the *in vivo* and *in vitro* localizations of [99mtechnicium] analogues.[18,23]

As a result of the extensive attention, the chemistry of rhenium organometallic complexes is well documented.[3-5,10,11,23-26] Rhenium was originally investigated due to its binding to DNA and RNA, which eventually led to its organometallic pharmaceutical development.[24] Due to having a wide range of oxidation states, -1 to +7, it has shown structural diversity, however the low oxidation states produce the more kinetically stable complexes as required in fluorescence imaging agents.[3,5]

The most common and studied[18,27-31] form of luminescent rhenium complexes belong to the family of *fac*-$[Re(CO)_3(diim)X]^{0/+}$, where diim is a bidentate diimine ligand such as 1,10-phenathroline (phen) and X is a monodentate anionic or neutral ancillary ligand such as chloride or pyridine.[32] These complexes have well documented photophysical properties that can be appropriately adjusted via the introduction of various functional groups into the diimine or ancillary ligand. Furthermore, chemical modification of these complexes can also be used to modulate their lipophilicity and optimize cellular uptake and cytotoxicity. *fac*-$[Re(CO)_3(diim)X]^{0/+}$ complexes have generally been shown to have low levels of cytotoxicity.[13] However in some cases, cytotoxic effects have been observed in a number of cell lines, although the specific mode of action for these species is not yet clearly elucidated.[33]

In our studies, we have investigated the cellular uptake and localization of neutral *fac*-[Re(CO)₃(phen)T] complexes, where T represent an aryltetrazolato ligand. These complexes localize in different organelles such as lipid droplets,[34] endoplasmic reticulum,[35] and acidic vesicles[34] depending of the specific substituent present on the tetrazolato ligand. For example, the rhenium species bound to 5-(4-cyanophenyl)-tetrazolate accumulates in lipid droplets with a high specificity for polar lipids such as phosphatidylethanolamine, cholesterol and sphingomyelin,[36] thus allowing visualization of polar lipid trafficking.[37] On the other hand, the rhenium species bound to 5-(pyrid-4-yl)-tetrazolate strongly located in the endoplasmic reticulum and allowed the visualization of membrane events in live cells.[35] These complexes were all found to be highly amenable to long term imaging in live cells and exhibited very low toxicity. The previous studies suggest that these rhenium tetrazolato complexes are kinetically inert and do not undergo ligand exchange reactions, at least before their specific targeted organelle is reached. This study therefore aimed to assess the stability of a transition metal complex after cellular incubation. For this scope, the complex *fac*-[Re(CO)₃(phen)L] was synthesized, where L is 5-(4-iodophenyl)-tetrazolate and the complex is herein referred to as **Re-I**. The aim is to combine confocal fluorescence microscopy alongside X-ray fluorescence imaging techniques to monitor the intracellular localization of the Re metal center and an I-labeled *p*-iodo-(tertazol-5-yl)-benzene ancillary ligand.
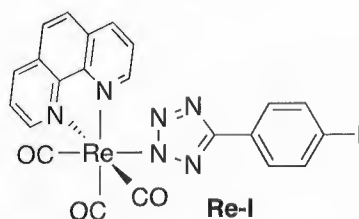
Figure 1. Structure of the investigated complex **Re-I**.

Experimental

Synthesis and Characterization

All reagents and solvents were purchased from Sigma Aldrich or Alfa Aesar. Nuclear magnetic resonance spectra were recorded using a Bruker Avance 400 spectrometer (400 MHz for ¹H NMR; 100 MHz for ¹³C NMR) at 300 K. All NMR spectra were calibrated to residual solvent signals. Infrared spectra were recorded using an attenuated total reflectance Perkin Elmer Spectrum 100 FT-IR with a diamond stage. IR spectra were recorded from 4000–650 cm⁻¹. The intensities of the band are reported as strong (s), medium (m), or weak (w), with broad (br) bands also specified. Melting

points were determined using a BI Barnsted Electrotermal 9100 apparatus. Elemental analysis were carried out on bulk samples using a Thermo Finning EA 1112 Series Flash.

Para-(Tetrazol-5-yl)-iodobenzene was prepared following the methodology described by Koguro.[38] Yield 57%. M.p. 268-269 °C (dec.). v_{max}/cm^{-1}: 2964 w, 2816 w, 2668 w, 2514 m, 2445 m, 1906 m, 1602 s, 1557 m, 1492 w, 1478 m, 1431 s, 1405 w, 1364 w, 1272 w, 1252 w, 1165 m, 1117 w, 1088 w, 1055 m, 1025 w, 1005 w, 81 s, 826 s, 742 m, 711 w, 693 w. ^{1}H-NMR δ/ppm (DMSO-d$_6$): 7.98 (2H, d, J = 8.4 Hz, Ph H2,6), 7.81 (2H, d, J = 8.4 Hz, Ph H3,5). ^{13}C-NMR δ/ppm (DMSO-d$_6$): 155.2 ($\underline{C}$N$_4$), 138.3, 128.7, 123.8, 98.4.

The synthesis of **Re-I** was performed according to the following procedure. *fac*-[Re(CO)$_3$(phen)Cl] (0.10 g, 0.2 mmol) was added to 10 mL of 3:1 a (v/v) ethanol/water solvent mixture. To this suspension, a solution obtained by dissolving *para*-(tetrazol-5-yl)-iodobenzene (1.6 eq.) and triethylamine (1.6 eq.) in 2.5 mL of 3:1 a (v/v) ethanol/water solvent mixture was added. The mixture was vigorously stirred and heated at reflux for 20 hr. After this time, the mixture was cooled to room temperature and filtered over a glass frit, affording the desired complex as yellow microcrystalline powder. Yield 95 %. M.p. 291.3-291.9 °C (dec.). Elemental analysis for C$_{22}$H$_{12}$IN$_6$O$_3$Re: calculated: C 36.62, H 1.68, N 11.65; found: C 36.43, H 1.44, N 11.46. v_{max}/cm^{-1}: 3798 w, 3060 w, 2023 s (CO, A$'$(1)), 1908 br s (CO, A$'$(2)/A$''$), 1631 w, 1600 w, 1584 w, 1425 m, 1411 m, 1338 w, 1269 w, 1226 w, 1177 w, 1146 w, 1117 w, 1038 w, 1000 w, 965 w, 848 w, 825 w, 779 w, 748 w, 721 w. ^{1}H-NMR δ/ppm (acetone-d$_6$): 9.65 (2H, d, J = 5.2 Hz, phen H2,9), 8.96 (2H, d, J = 8.2 Hz, phen H4,7), 8.30 (2H, s, phen H5,6), 8.19-8.15 (2H, m, phen H3,8), 7.62 (2H, d, J = 8.4 Hz, Ph H3,5), 7.43 (2H, d, J = 8.8 Hz, Ph H2,6). ^{13}C-NMR δ/ppm (acetone-d$_6$): 162.9 ($\underline{C}$N$_4$), 155.2, 148.3, 140.4, 138.4, 131.7, 130.9, 128.7, 128.6, 127.4, 93.9. Crystals suitable for X-ray analysis were obtained by liquid-liquid diffusion of petroleum spirits into a dichloromethane solution of **Re-I** (see SI).

Photophysical Measurements

Absorption spectra were recorded at room temperature using a Cary 4000 UV/Vis spectrometer. Uncorrected steady state emission and excitation spectra were recorded on an Edinburgh FLSP980-S2S2-stm spectrometer equipped with: i) a temperature-monitored cuvette holder; ii) 450 W Xenon arc lamp; iii) double excitation and emission monochromators; iv) a Peltier cooled Hamamatsu R928P photomultiplier tube (spectral range 200-870 nm). Emission and excitation spectra were corrected for source intensity (lamp and grating) and emission spectral response (detector and grating) by a calibration curve supplied with the instrument. According to the approach described by Demas and Crosby,[39] luminescence quantum yields (Φ_{em}) were measured in optically dilute solutions (O.D. < 0.1 at excitation wavelength) obtained from absorption spectra on a wavelength scale [nm] and compared to the reference emitter by the following equation:

$$\Phi_x = \Phi_r \left[\frac{A_r(\lambda_r)}{A_x(\lambda_x)} \right] \left[\frac{I_r(\lambda_r)}{I_x(\lambda_x)} \right] \left[\frac{n_x^2}{n_r^2} \right] \left[\frac{D_x}{D_r} \right]$$

where A is the absorbance at the excitation wavelength (λ), I is the intensity of the excitation light at the excitation wavelength (λ), n is the refractive index of the solvent, D is the integrated intensity of the luminescence and Φ is the quantum yield. The subscripts r and x refer to the reference and the sample, respectively. The quantum yield determinations were performed at identical excitation wavelength for the sample and the reference, therefore cancelling the $I(\lambda_r)/I(\lambda_x)$ term in the equation. The quantum yields of complexes were measured against an aqueous solution of [Ru(**bipy**)$_3$]Cl$_2$ (**bipy** = 2,2'-bipyridine; Φ_r = 0.028).[40] Emission lifetimes (τ) were determined with the time correlated single photon counting technique (TCSPC) with the same Edinburgh FLSP980-S2S2-stm spectrometer using either a pulsed picosecond LED (EPLED/EPL 377 nm, FHWM < 800 ps). The goodness of fit was assessed by minimising the reduced χ^2 function and by visual inspection of the weighted residuals. The dichloromethane solvent used for the preparation of the solutions for the photophysical investigations were of LR grade. Degassing of the dichloromethane solution was performed using the freeze-pump-thaw method. Experimental uncertainties are estimated to be ±8% for lifetime determinations, ±20% for quantum yields, ±2 nm and ±5 nm for absorption and emission peaks, respectively.

Cell Culture

22Rv1 human prostate epithelial carcinoma cells, originally purchased from the European Collection of Cell Cultures via CellBank Australia (Children's Medical Research Institute, New South Wales Australia), were cultured as monolayers in complete RPMI-1640 (Sigma Life Sciences) supplemented with foetal bovine serum (10% v/v; Invitrogen Australia, Thermo-Fischer Scientific), L-glutamine (2 mM, Sigma Life Sciences), antibiotic-antimyotic mixture (100 mg.mL-1 penicillin and 100 U.mL^{-1} streptomycin; Sigma Life Sciences) at 310 K in a 5% CO$_2$-humidified incubator and were sub-cultured every 3-4 days.

*Preparation of **Re-I** Treatment Solutions*

Re-I was dissolved in DMSO to produce a 10 mM solution. This solution was then diluted with PBS to the treatment concentration of 10 μM (0.1% DMSO).

Cell Treatment Sample Preparations

Cells were prepared for XRF imaging by growth on 1.5 x 1.5 mm x 500 nm silicon nitride windows (Silson, UK) in 6-well plates as described previously.[41-46] The plates were seeded at 1 x 10^6 cells/well in complete DMEM and were incubated at 310 K in a 5% CO$_2$-humidified incubator for 24 hrs prior

to treatment. Cells were then treated with **Re-I** or DMSO (0.1%) as a vehicle-only control for 2 hr. At the end of the treatment time the medium was removed and cells were fixed with 3.7% paraformaldehyde (prepared fresh in PBS) solution for 15 mins. Fixed windows were then washed with PBS, ammonium acetate (in Milli-Q water) and Milli-Q water thrice. (Procedure adapted from references [47,48])

Spectroscopic Data Collection

Confocal fluorescence images were collected with an Olympus BX53 upright fluorescence microscope (Olympus, Australia), with a 10x lens and excitation wash with a blue LED and images were collected in bright field mode or using a long band pass filter.

XRF elemental distribution maps of single cells were recorded on beamline 2-ID-D at the Advanced Photon Source (APS), Argonne National Laboratory, Illinois, USA. The X-ray beam was tuned to an incident energy of 12.7 keV using a beam splitting Si(220) monochromator and was focused to a diameter of ~0.25 μm using a "high-flux" zone plate. A single element silicon drift energy dispersive detector (Vortex EX, SII Nano- technology, Northridge, CA), at 90° to the incident beam, was used to collect the fluorescence signal for 1 s per spatial point from samples under a He atmosphere.

Four to eight individual cells per sample were selected and located using an optical microscope (Leica DMRXE). Cells were subsequently relocated in the beamline by correlating the light microscope coordinates with those determined from the X-ray transmission image of the window as viewed on a CCD camera. Whole cells were raster scanned using a 25 nm accuracy Newport sample positioning stage. Low resolution scans with a step size of 4 μm and a dwell time of 0.5 s were used to locate the cells before obtaining high-resolution scans with a step size of 0.5 μm and a dwell time of 1 s.

XFM Data Analysis

The fluorescence spectrum at each spatial point was fit to Gaussians, modified by the addition of a step function and a tailing function to describe mostly incomplete charge collection and other detector artefacts.[49,50] The integrated fluorescence spectra extracted from these regions were also fit with modified Gaussians to determine average elemental area densities (in units of μg cm^{-2}). Quantification was performed by comparison to the corresponding measurements on the thin-film standards NBS-1832 and NBS-1833 from the National Bureau of Standards (Gaithersburg, MD). The analysis was performed using MAPS software.[42,50]

Results

The complex **Re-I** was obtained via a direct ligand exchange reaction between the chloro ligand in *fac*-[Re(CO)$_3$(phen)Cl] with the tetrazolate anion. Compared to previously investigated methodologies, involving the preparation of the intermediate complex *fac*-[Re(CO)$_3$(phen)(NCCH$_3$)],[51] the direct exchange yields the targeted compound in high purity without the need of chromatographic purification. The species **Re-I** displays the expected peaks belonging to the CO ligands at 2023 and 1908 cm^{-1} in the IR spectrum, as typical for rhenium tetrazolato complexes of *facial* configuration.[51] The formulation of **Re-I** was further supported by NMR and elemental analysis. Single crystals suitable for X-ray diffraction could be obtained by layering petroleum spirits onto a dichloromethane solution of the complex. The obtained structure (see SI) highlights the expected rhenium complex coordinated by three *facial* CO ligands, a chelating phen and the N2 coordinated tetrazolato ligand.

The photophysical data for **Re-I** from a diluted dichlorometane solution are reported in Table 1, and the relative absorption, excitation, and emission spectra are reported in the SI. As expected for this class of rhenium complexes,[51] the absorption profile presents an intense band in the 250-310 nm region originating from ligand centered (LC) $\pi\pi^*$ transitions on the phen and tetrazolato ligands. A further band of lower intensity is visible in the 310-420 nm region, typical of metal-to-ligand charge transfer transitions (MLCT) partially mixed with ligand-to-ligand charge transfer character (LLCT). Upon excitation to the charge transfer manifold, **Re-I** exhibits an emission profile that is broad and structure-less with a maximum at 590 nm. The elongation of the excited state lifetime (τ) from 0.262 to 0.591 µs upon degassing, along with an increase of the photoluminescence quantum yield (Φ), support the triplet spin multiplicity of the excited state (^{3}MLCT).

Table 1. Photophysical data for **Re-I** from diluted (*ca* 10^{-5} M) dichloromethane solutions.

Absorption: λ_{max}/nm (ε/10^{4}M^{-1}cm^{-1})	267 (5.15), 365 (0.50)
Emission - 298 K: λ_{max}/nm	590
Air-equilibrated - 298 K: τ/µs	0.262
Deareated - 298 K: τ/µs	0.591
Air-equilibrated Φ	0.028
Deareated Φ	0.083
k_r/10^{6}s^{-1}	0.14

$k_{nr}/10^6 s^{-1}$	1.55

Cellular uptake and distribution of **Re-I** was investigated using confocal fluorescence and X-ray fluorescence microscopy. 22Rv1 cells were grown on silicon nitride windows overnight before being treated with **Re-I** for 2 and 4 hrs. After incubation, the cells were fixed in paraformaldehyde and freeze dried before imaging. The use of paraformaldehyde as a fixative agent is known to preserve the morphology of cells for confocal and XFM imaging.[43,44,52] The optical fluorescence of the entire window was imaged and stitched together immediately after fixation. Samples were then transported to the Advanced Photon Source (APS), Argonne National Laboratory, Illinois, USA for subsequent XFM imaging.

The zinc (Zn) map was used to identify the approximate boundaries of the cells as this element showed consistently higher signal-to-noise ratio (Fig. 1). The synchrotron beam at 12.7 keV was focused to 1 μm and then raster scanned to simultaneously obtain elemental maps of individual cells. As the beam moved across the cells the resulting fluorescence spectrum at each dwell point was collected and formed a single pixel within the elemental map.

Elemental maps were obtained for typically important biological elements (P, S, Cl, K, Ca) as well as transition metals (Fe, Zn). Rhenium concentrations were below detection limit within the control
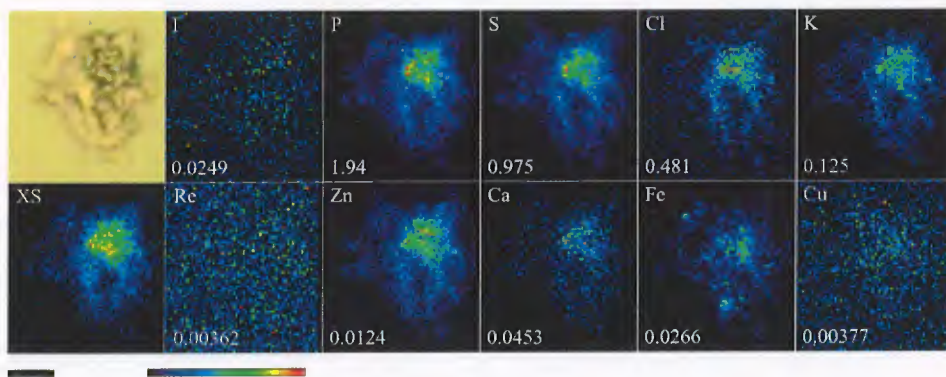
cells (Fig. 1), – no Re-based fluorescence signal was observed nor any definable cellular localization. Likewise, iodine was only found to be present in extremely low native concentrations in the control cells, with a very poorly defined intracellular distribution.

Figure 1 – Optical micrograph (top left), scattered X-ray (XS) and XFM elemental distribution maps of a 22Rv1 control cell. The maximum elemental area densities (quantified from standards and

expressed in micrograms per square centimetre) are given in the bottom corner of each map. The scale bar represents 10 μm.

All cells treated with **Re-I** showed elemental concentrations localized within the cell, with notable exceptions for rhenium, iodine and zinc, which were also occasionally found outside the boundaries of the cell (Fig. 2). The co-localisation of rhenium and iodine, both inside and outside the cells, is consistent with the fact that the tetrazolato ancillary ligand has not dissociated from the rhenium center. The cellular uptake of **Re-I** is still clearly visible by strong intracellular concentrations of both rhenium and iodine within all treated cells.

The **Re-I** complex appeared to strongly adhere to the silicon nitride windows such that extracellular localizations of rhenium and iodine were visible (Fig. 2). These spots were also fluorescent, identifying them to be from adhered complex, however the co-localization with zinc is unusual. Zinc, while not part of the complexes structure, was the only element to be additionally co-localized both within the cell and in the spots where the **Re-I** complex adhered.

The intense regions of the optical fluorescence images were visually similar to the rhenium intracellular distribution from XFM imaging, indicating that the luminescence detected by confocal microscopy was likely to be originating from **Re-I**. Taken together with the similarity of the XFM maps of rhenium and iodine distributions, this supports the interpretation that the complex was still intact at the time of XFM imaging. This is in line with the theory that the low spin d^6 complexes form kinetically stable complexes, even in complex biological systems.

If the ancillary ligand had dissociated from **Re-I,** it would likely display a more localised cellular distribution than that observed in the optical or XFM imaging. Presumably, its planar, aromatic nature would result in the free ligand accumulating in lipid layers as well as potentially intercalating within DNA in the nucleus.[53]
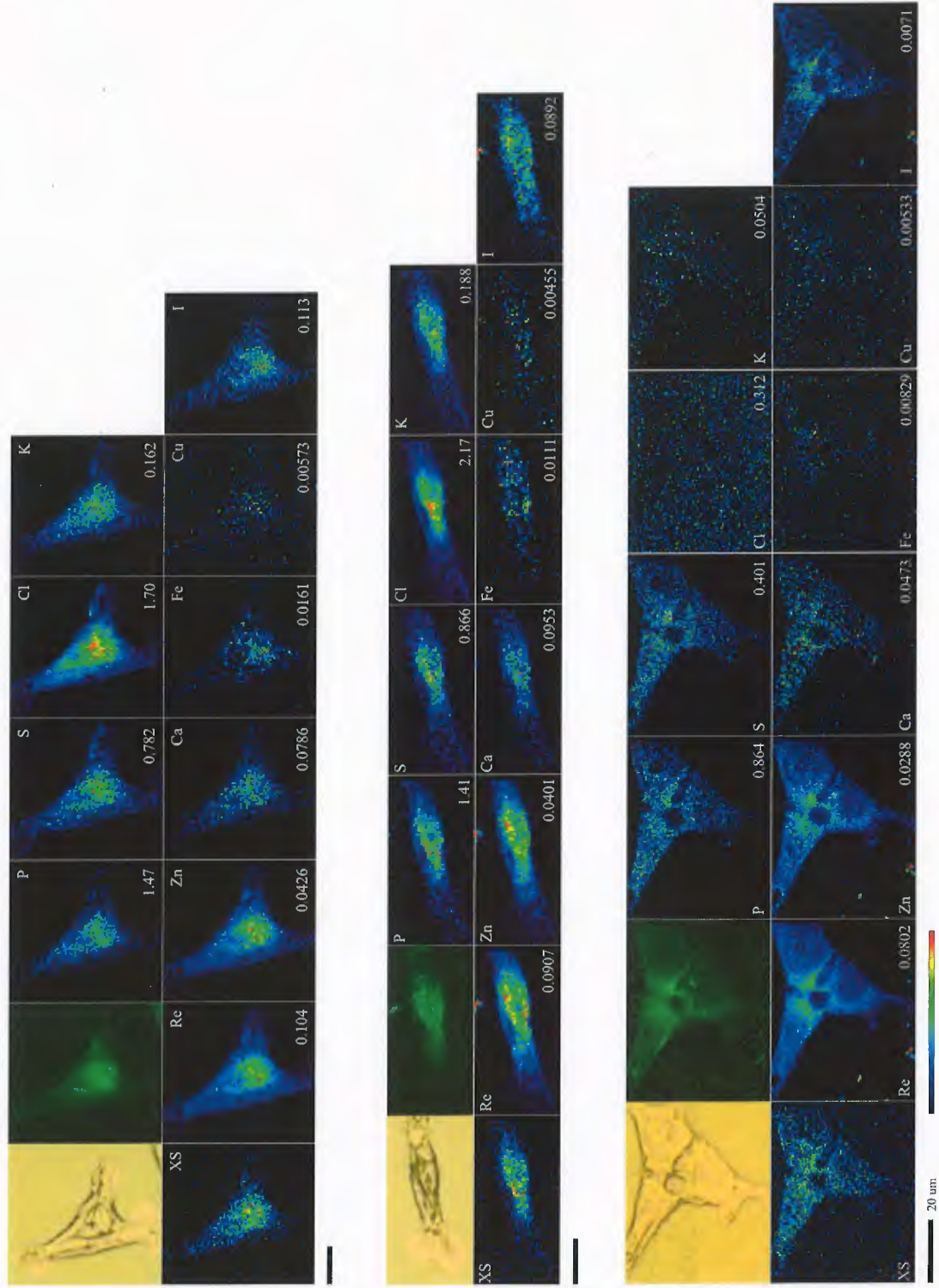
Figure 2 – Optical micrographs (top left), confocal fluorescence microscopy images (second right, top), scattered X-ray (XS) and XFM elemental

distribution maps of 22Rv1 cells treated with **Re–I** for 2 hr (top, middle) or 4 hr (bottom). The maxima elemental area densities (quantified from standards and expressed in micrograms per square centimeter) are given in the bottom corner of each map. The black bar under the maps represents 10 μm unless otherwise indicated.

The distribution of Re-I in the 22Rv1 cell is consistent with the staining of a diffuse reticular network in the nuclear/perinuclear region. Where the nuclear regions of the cells were identified using the P and Zn maps, given the inherently higher concentrations of phosphate from the DNA backbone and Zn from zinc finger proteins within the nucleus.[48] The exchange of a nitrile functional group for iodine in *fac*-[Re(CO)₃(phen)T], where T is 5-(4-cyanophenyl)tetrazolato, has unsurprisingly not appreciably altered the biological behavior of the rhenium complex inside the cells. The nitrile derivative was previously shown to have high affinity for polar lipids,[36] and the localization of Re-I within the reticular network may also suggest an affinity for lipids; the endoplasmic reticulum is an important manufacturing site for lipids. The distribution of **Re-I** does follow the thickness of the cell (Fig. 3) but this is as expected; 22Rv1s are a relatively thin cell where the vast majority of cellular organization is localized around the nucleus. Localization within the diffuse reticular network of the endoplasmic reticulum has been previously reported with other rhenium tetrazolato complexes in live HeLa cells[54] as well as with larger more complex ancillary biomolecules, such as nuclear,[21] peri-nuclear,[15] cytoplasmic[17] and cellular compartments,[14] and some organelle[18] specific distributions. Three-colour elemental correlation images readily identified strong extracellular colocalisations of rhenium, iodine and zinc (Fig. 4).

Figure 3 – XRF elemental distribution maps for a 22Rv1 cell incubated with **Re-I** for
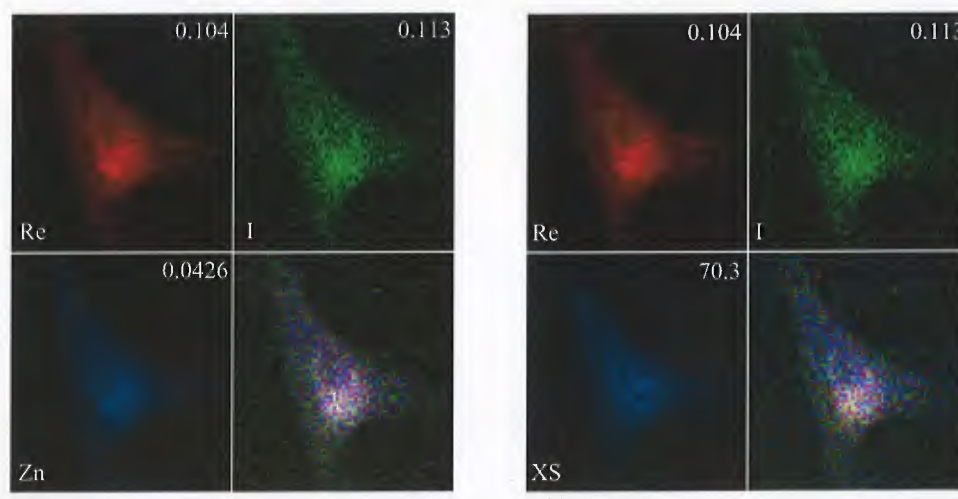
2 hr showing the colocalisation of rhenium (red), iodine (green) and zinc (blue) (left), cell thickness (blue, XS) (right), and the resultant three-colour overlay; where white indicates co-localisation of all three elements. The maximum elemental area densities

(quantified from standards and expressed in micrograms per square centimeter) are given in the top corner of each map. The scale bar represents 10 μm.
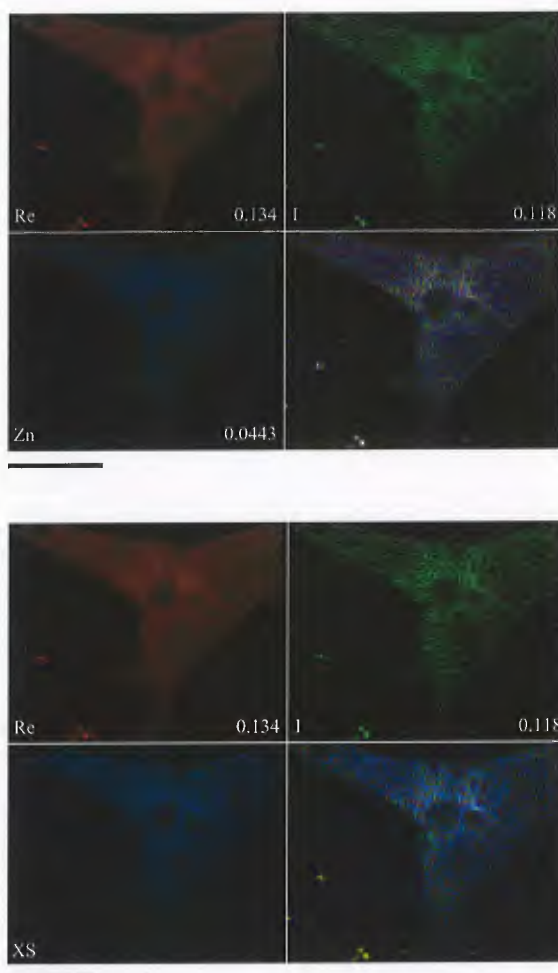

Figure 4 – XRF elemental distribution maps for a 22Rv1 cell incubated with **Re-I** for 4 hr showing the colocalisation of rhenium (red), iodine (green) and zinc (blue) (top), cell thickness (blue, XS) (bottom), and the resultant three-colour overlay; where white indicates co-localisation of all three elements. The maximum elemental area densities (quantified from standards and expressed in micrograms per square centimeter) is given in the top corner of each map. The scale bar represents 20 μm.

From the XFM data the total average rhenium content can be quantified for both the cell as a whole and related to an area designated as nuclear fractions (Fig. 5). The quantitation of cellular elemental content showed a significant increase in both rhenium and iodine concentrations between control and treated cells. Furthermore, the ratio of cell to nuclear content for rhenium is consistent with data which shows **Re-I** and its

cyanophenyl analogue having preferential localization to cytoplasmic areas around the nucleus. It should be noted that the quantitation of elemental contents in the nuclear regions of the cell also includes elemental content in over- or underlying structures, e.g. the endoplasmic reticulum, because the XFM images are simply two-dimensional projections of (dried) three-dimensional objects. There was no significant increase in intracellular contents of either rhenium or iodine in treated cells between the 2 and 4 hr incubation periods, indicating that a 2 hr treatment was sufficient to allow uptake. The ratio of the total cellular contents (as masses) for rhenium and iodine were observed to be approximately in concordance with the ratio of their atomic masses and the expected 1:1 stoichiometric ratio, again providing some evidence to support the kinetic stability of the complex after cellular uptake.

Homeostasis of some other biologically relevant elements was disrupted by incubation with **Re-I** with significant changes in intracellular content of selenium, chlorine, zinc and potassium. However, not all elements were similarly affected, for example there was a general increase in zinc content for both the 2 and 4 hr treatments; whereas potassium only saw significant increases with the 2 hr treatment. Furthermore, some elements saw no significant change to their content levels, such as sulfur and iron. This might provide a very important way of assessing the impact of imaging agents on cells by identifying subtle changes in cellular metabolism/homeostasis.
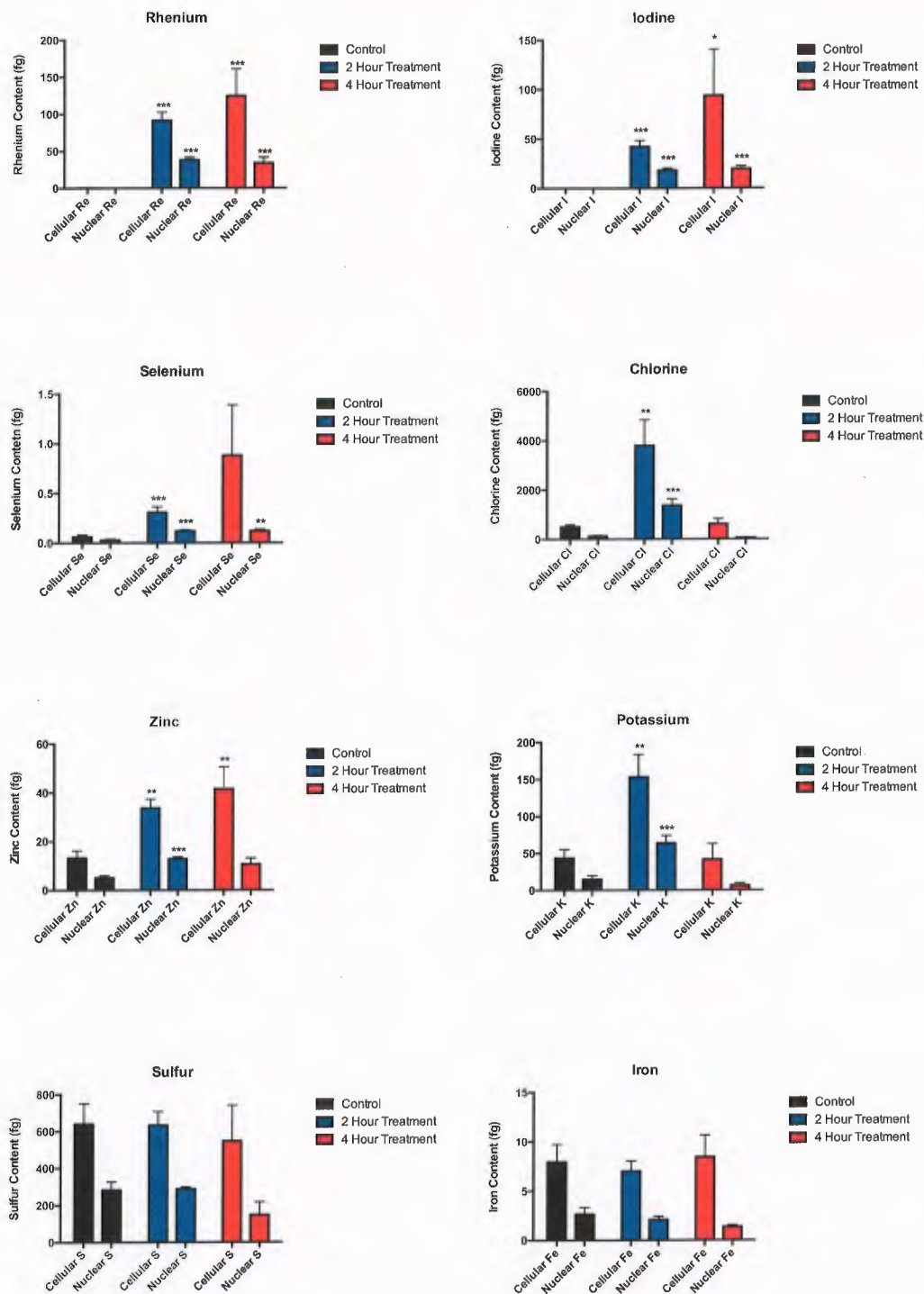
Figure 5 – Intracellular content of rhenium and other biologically relevant elements within 22Rv1 cells treated with fluorescent complex **Re-I** as quantified by XFM studies. * Represents p<0.1, ** p<0.05, *** p<0.005 for comparisons between controls and treated cells.

Conclusions

In this study we have demonstrated that the cellular distribution a novel Re(I) based luminescent imaging agent can be determined by monitoring the luminescence from the compound using optical microscopy and then correlated with the cellular distributions of Re and I contained in the species within the same samples as measured using microprobe X-ray fluorescence imaging.

The iodinated tetrazolato ancillary group on the complex resulted in a similar cellular distribution within the 22Rv cell line to that reported for a related *fac*-[Re(CO)$_3$(phen)T], where T is 5-5-(pyrid-4-yl)-tetrazolate, which interacts with endoplasmic reticulum. The intracellular distribution of **Re-I** therefore approximately followed the cell thickness producing a diffuse reticular network staining pattern.

The combination of optical microscopy with XFM imaging was able to provide more information beyond just the distribution of the complex. A co-localisation of zinc with the exogenous elements was evident both inside and outside of the cells. Quantitation of cellular elemental contents arising from integrated XFM signals showed that the homeostasis of some biological elements was disrupted by treatment with **Re-I** and that this may be used to identify subtle impacts of imaging agents on cellular homeostasis. The principal conclusion drawn from the XFM imaging study was based on the observation that the distributions of rhenium and iodine were very similar, which indicated that the complex remained intact in the cells after uptake.

References

1. R. G. Balasingham, M. P. Coogan and F. L. Thorp-Greenwood, *Dalton Trans.*, 2011, **40**, 11663-11674.
2. V. Fernandez-Moreira, F. L. Thorp-Greenwood and M. P. Coogan, *Chem. Commun.*, 2010, **46**, 186-202.
3. S. Prakash, M. J. Went and P. J. Blower, *Nucl. Med. Biol.*, 1996, **23**, 543-549.
4. W. A. Volkert and T. J. Hoffman, *Chem. Rev.*, 1999, **99**, 2269-2292.
5. L. H. Wei, J. W. Babich, W. Ouellette and J. Zubieta, *Inorg. Chem.*, 2006, **45**, 3057-3066.
6. A. Carreno, M. Gacitua, J. A. Fuentes, D. Paez-Hernandez, J. P. Penaloza, C. Otero, M. Preite, E. Molins, W. B. Swords, G. J. Meyer, J. M. Manriquez, R. Polanco, I. Chavez and R. Arratia-Perez, *New J. Chem.*, 2016, **40**, 7687-7700.
7. M. P. Coogan and V. Fernandez-Moreira, *Chem. Commun.*, 2014, **50**, 384-399.
8. M. Patra and G. Gasser, *ChemBioChem*, 2012, **13**, 1232-1252.
9. V. Sathish, E. Babu, A. Ramdass, Z. Z. Lu, M. Velayudham, P. Thanasekaran, K. L. Lu and S. Rajagopal, *Talanta*, 2014, **130**, 274-279.
10. S. R. Banerjee, L. H. Wei, M. K. Levadala, N. Lazarova, V. O. Golub, C. J. O'Connor, K. A. Stephenson, J. F. Valliant, J. W. Babich and J. Zubieta, *Inorg. Chem.*, 2002, **41**, 5795-5802.
11. R. Alberto, R. Schibli, R. Waibel, U. Abram and A. P. Schubiger, *Coordin. Chem. Rev.*, 1999, **192**, 901-919.
12. S. T. Lam, N. A. Y. Zhu and V. W. W. Yam, *Inorg. Chem.*, 2009, **48**, 9664-9670.
13. K. K. W. Lo, *Accounts Chem. Res.*, 2015, **48**, 2985-2995.
14. A. J. Amoroso, M. P. Coogan, J. E. Dunne, V. Fernandez-Moreira, J. B. Hess, A. J. Hayes, D. Lloyd, C. Millet, S. J. A. Pope and C. Williams, *Chem. Commun.*, 2007, DOI: 10.1039/b706657k, 3066-3068.
15. R. G. Balasingham, F. L. Thorp-Greenwood, C. F. Williams, M. P. Coogan and S. J. A. Pope, *Inorg. Chem.*, 2012, **51**, 1419-1426.
16. C. Y. Li, M. X. Yu, Y. Sun, Y. Q. Wu, C. H. Huang and F. Y. Li, *J. Am. Chem. Soc.*, 2011, **133**, 11231-11239.
17. K. K. W. Lo, A. W. T. Choi and W. H. T. Law, *Dalton Trans.*, 2012, **41**, 6021-6047.
18. E. E. Langdon-Jones, N. O. Symonds, S. E. Yates, A. J. Hayes, D. Lloyd, R. Williams, S. J. Coles, P. N. Horton and S. J. A. Pope, *Inorg. Chem.*, 2014, **53**, 3788-3797.
19. P. Hafliger, N. Agorastos, B. Spingler, O. Georgiev, G. Viola and R. Alberto, *ChemBioChem*, 2005, **6**, 414-421.
20. K. P. Maresca, S. M. Hillier, F. J. Femia, C. N. Zimmerman, M. K. Levadala, S. R. Banerjee, J. Hicks, C. Sundararajan, J. Valliant, J. Zubieta, W. C. Eckelman, J. L. Joyal and J. W. Babich, *Bioconjugate Chem.*, 2009, **20**, 1625-1633.

21. V. Polyakov, V. Sharma, J. L. Dahlheimer, C. M. Pica, G. D. Luker and D. Piwnica-Worms, *Bioconjugate Chem.*, 2000, **11**, 762-771.
22. M. Sagnou, S. Tzanopoulou, C. P. Raptopoulou, V. Psycharis, H. Braband, R. Alberto, I. C. Pirmettis, M. Papadopoulos and M. Pelecanou, *Eur. J. Inorg. Chem.*, 2012, DOI: 10.1002/ejic.201200450, 4279-4286.
23. D. J. Kramer, A. Davison, W. M. Davis and A. G. Jones, *Inorg. Chem.*, 2002, **41**, 6181-6183.
24. R. H. Fish and G. Jaouen, *Organometallics*, 2003, **22**, 2166-2177.
25. T. W. Spradau and J. A. Katzenellenbogen, *Bioconjugate Chem.*, 1998, **9**, 765-772.
26. S. Top, A. Vessieres and G. Jaouen, *J. Chem. Soc.-Chem. Comm.*, 1994, DOI: DOI 10.1039/c39940000453, 453-454.
27. A. El Nahhas, A. Cannizzo, F. van Mourik, A. M. Blanco-Rodriguez, S. Zalis, A. Vlcek and M. Chergui, *J Phys. Chem. A*, 2010, **114**, 6361-6369.
28. P. J. Giordano and M. S. Wrighton, *J. Am. Chem. Soc.*, 1979, **101**, 2888-2897.
29. T. M. McLean, J. L. Moody, M. R. Waterland and S. G. Telfer, *Inorg. Chem.*, 2012, **51**, 446-455.
30. D. K. Orsa, G. K. Haynes, S. K. Pramanik, M. O. Iwunze, G. E. Greco, D. M. Ho, J. A. Krause, D. A. Hill, R. J. Williams and S. K. Mandal, *Inorg. Chem. Commun.*, 2008, **11**, 1054-1056.
31. R. Schibli and P. A. Schubiger, *Eur. J. Nucl. Med. Mol. Imag.*, 2002, **29**, 1529-1542.
32. R. A. Kirgan, B. P. Sullivan and D. P. Rillema, *Journal*, 2007, **281**, 45-100.
33. A. Leonidova and G. Gasser, *ACS Chem. Biol.*, 2014, **9**, 2180-2193.
34. C. A. Bader, R. D. Brooks, Y. S. Ng, A. Sorvina, M. V. Werrett, P. J. Wright, A. G. Anwer, D. A. Brooks, S. Stagni, S. Muzzioli, M. Silberstein, B. W. Skelton, E. M. Goldys, S. E. Plush, T. Shandala and M. Massi, *RSC Adv.*, 2014, **4**, 16345-16351.
35. C. A. Bader, A. Sorvina, P. V. Simpson, P. J. Wright, S. Stagni, S. E. Plush, M. Massi and D. A. Brooks, *FEBS Lett.*, 2016, **590**, 3051.
36. C. A. Bader, E. A. Carter, A. Safitri, P. V. Simpson, P. Wright, S. Stagni, M. Massi, P. A. Lay, D. A. Brooks and S. E. Plush, *Mol. Biosyst.*, 2016, **12**, 2064-2068.
37. C. A. Bader, T. Shandala, E. A. Carter, A. Ivask, T. Guinan, S. M. Hickey, M. V. Werrett, P. J. Wright, P. V. Simpson, S. Stagni, N. H. Voelcker, P. A. Lay, M. Massi, S. E. Plush and D. A. Brooks, *PloS One*, 2016, **11**.
38. K. Koguro, T. Oga, S. Mitsui and R. Orita, *Synthesis*, 1998, 910-914.
39. J. N. Demas and G. A. Crosby, *J. Phys. Chem.*, 1971, **75**, 991-1024.
40. K. Nakamaru, *B. Chem. Soc. Jpn.*, 1982, **55**, 2697-2705.
41. J. B. Aitken, S. Antony, C. M. Weekley, B. Lai, L. Spiccia and H. H. Harris, *Metallomics*, 2012, **4**, 1051-1056.
42. E. A. Carter, B. S. Rayner, A. I. McLeod, L. E. Wu, C. P. Marshall, A. Levina, J. B. Aitken, P. K. Witting, B. Lai, Z. H. Cai, S. Vogt, Y. C. Lee, C. I. Chen, M. J. Tobin, H. H. Harris and P. A. Lay, *Mol. Biosyst.*, 2010, **6**, 1316-1322.
43. C. M. Weekley, J. B. Aitken, S. Vogt, L. A. Finney, D. J. Paterson, M. D. de Jonge, D. L. Howard, I. F. Musgrave and H. H. Harris, *Biochemistry*, 2011, **50**, 1641-1650.

44. C. M. Weekley, J. B. Aitken, S. Vogt, L. A. Finney, D. J. Paterson, M. D. de Jonge, D. L. Howard, P. K. Witting, I. F. Musgrave and H. H. Harris, *J. Am. Chem. Soc.*, 2011, **133**, 18272-18279.

45. C. M. Weekley, G. Jeong, M. E. Tierney, F. Hossain, A. M. Maw, A. Shanu, H. H. Harris and P. K. Witting, *J. Biol. Inorg. Chem.*, 2014, **19**, 813-828.

46. C. M. Weekley, A. Shanu, J. B. Aitken, S. Vogt, P. K. Witting and H. H. Harris, *Metallomics*, 2014, **6**, 1602-1615.

47. R. McRae, B. Lai and C. J. Fahrni, *Metallomics*, 2013, **5**, 52-61.

48. R. McRae, B. Lai, S. Vogt and C. J. Fahrni, *J. Struct. Biol.*, 2006, **155**, 22-29.

49. P. Van Espen, eds. R. E. Van Grieken and A. A. Markowicz, CRC Press, 2nd edn., 2002, vol. 29.

50. S. Vogt, *J. Phys. IV*, 2003, **104**, 635-638.

51. M. V. Werrett, D. Chartrand, J. D. Gale, G. S. Hanan, J. G. MacLellan, M. Massi, S. Muzzioli, P. Raiteri, B. W. Skelton, M. Silberstein and S. Stagni, *Inorg. Chem.*, 2011, **50**, 1229-1241.

52. C. M. Weekley, J. B. Aitken, L. Finney, S. Vogt, P. K. Witting and H. H. Harris, *Nutrients*, 2013, **5**, 1734-1756.

53. L. P. G. Wakelin, *Med. Res. Rev.*, 1986, **6**, 275-340.

54. M. V. Werrett, P. J. Wright, P. V. Simpson, P. Raiteri, B. W. Skelton, S. Stagni, A. G. Buckley, P. J. Rigby and M. Massi, *Dalton Trans.*, 2015, **44**, 20636-20647.